Journal of
Ceramic Science
and Technology

J. Ceram. Sci. Tech., **05** [03] 237-244 (2014)
DOI: 10.4416/JCST2014-00013
available online at: http://www.ceramic-science.com

Solid Solutions and Thermal Transformations in Nanosized $LaPO_4$-YPO_4-H_2O and $LaPO_4$-$LuPO_4$-H_2O Systems

L. Mezentseva*[1], A. Osipov[1], V. Ugolkov[1], I. Kruchinina[1, 2], V. Popova[1], A. Yakovlev[1], T. Maslennikova[1]

[1]Grebenshchikov Institute of Silicate Chemistry, Russian Academy of Sciences, Makarova emb., 2, Saint-Petersburg, 199034, Russian Federation
[2]Saint-Petersburg Electrotechnical University "LETI", ul. Prof. Popova 5, 197376, Saint-Petersburg, Russian Federation

received April 11, 2014; received in revised form June 2, 2014; accepted July 11, 2014

Abstract

Nanosized powders of orthophosphates in the $LaPO_4$-YPO_4(-H_2O) and $LaPO_4$-$LuPO_4$-H_2O systems are synthesized to increase the mutual solubility of $LaPO_4{\cdot}nH_2O$, $YPO_4{\cdot}nH_2O$ and $LuPO_4{\cdot}nH_2O$ initial components and to investigate physicochemical properties of nanosized solid solutions and their mixtures. The temperature dependence of nanoparticle size is investigated in the 200 – 1100 °C temperature range. Formation of limited hexagonal, monoclinic or tetragonal solid solutions is revealed, and the limits of their concentration and thermal stability are determined. In the $LaPO_4$-YPO_4(-H_2O) system a series of limited hexagonal $LaPO_4{\cdot}nH_2O$-based solid solutions is observed up to 500 – 600 °C within the $0 \le x \le 0.5$ concentration range; a monoclinic $LaPO_4$-based form is observed up to at least 1000 °C within the $0 \le x \le 0.7$ concentration range. Melting temperatures of $La_{1-x}Y_xPO_4$ samples are found to be in the 2010 – 1960 °C temperature range. In the $LaPO_4$-$LuPO_4$-H_2O system corresponding hexagonal solid solutions are observed within the $0 \le x \le 0.4$ concentration range; isomorphic capacity of the monoclinic form at 1100 °C is between 20 – 25 mol%. Solubility of $LaPO_4$ in tetragonal YPO_4 or $LuPO_4$ in all cases is less than 10 mol%. The specific surface area of $La_{1-x}Lu_xPO_4{\cdot}nH_2O$ powders is in the range of 46.7 – 90.3 m^2/g depending on x.

Keywords: $LaPO_4$-YPO_4-H_2O and $LaPO_4$-$LuPO_4$-H_2O systems, nanopowders, thermal behavior

I. Introduction

Rare earths orthophosphates are attracting considerable interest from researchers because of their unique properties and are now widely investigated. They are considered prospective catalysts for the oxidative dehydrogenation of ethylbenzene [1], iso-butane to iso-butene [2,3], as scintillators, laser hosts, and thermophosphors [4,5,6]. In addition, ceramics based on rare earth orthophosphates exhibit promising properties owing to their machinability [7,8,9] and high thermal and radiation stability and could be considered as matrices for radioactive waste immobilization (radioactive rare earth elements or trivalent actinides) [10,11,12,13]. Efficiency of such ceramic matrices is based on high isomorphic capacity in relation to immobilized elements. The main requirements for a ceramic matrix are formation of stable compositions with immobilized elements and high isomorphic capacity. In this connection the influence of nanoscale on mutual solubility of rare earths orthophosphates and other properties appears to be dramatic.

Rare earth orthophosphate nanopowders obtained with the sol-gel technique (precipitation from water solution) were used within the framework of preparation and investigation of properties of the ceramics. $LaPO_4$-$LuPO_4$-H_2O and $LaPO_4$-YPO_4-H_2O were chosen as modeling systems, where components belong to different structural groups (hexagonal $LaPO_4{\cdot}nH_2O$ or monoclinic $LaPO_4$ and tetragonal $YPO_4{\cdot}nH_2O$ and $LuPO_4{\cdot}nH_2O$ or YPO_4·and $LuPO_4$) [14].

Rare earth orthophosphate nanoparticles have often been synthesized by means of various modifications of sol-gel method. Analysis of the data presented in [15,16,17,18] has demonstrated that hydrated orthophosphates of rare-earth elements (REE) and their solid solutions are formed at stoichiometric ratio of interacting components ($Ln(NO_3)_3$ and $NH_4H_2PO_4$, $(NH_4)_2HPO_4$ or H_3PO_4) in an aqueous solution in the form of stable colloids that coagulate at pH ≈ 7.

The hydrated REE orthophosphates (La to Dy), which crystallize in a hexagonal system upon precipitation contain 0.5 – 3 moles of H_2O per formula unit. These compounds are the analogues of rhabdophane, they lose water molecules on being heated up to 450 – 600 °C and then transform into monazite-type monoclinic form [11,15,17,18,19,20]. The dehydration of other REE orthophosphates (Ho-Lu, Y, Sc) takes place in the 150 – 450 °C temperature range with the complete removal of water. According to the data presented in [15,16,21], the

* Corresponding author: la_mez@mail.ru

dehydration does not bring about structural transformations, i.e. the compounds retain the xenotime structure.

According to our previous investigation [22], mutual solubility of RE orthophosphates belonging to different structural groups, whose particles have the micron size, is insignificant and makes up 2 – 3 mol% from each side (for instance, in the $LaPO_4$-$YbPO_4$ system the limited solid solutions have the following compositions - $La_{0.98}Yb_{0.02}PO_4$ (monoclinic) and $La_{0.03}Yb_{0.97}PO_4$ (tetragonal)). In the $LaPO_4$-YPO_4 system, according to [23], solubility of tetragonal YPO_4 in monoclinic $LaPO_4$ at 1200 °C ranges up to 20 mol%. Tetragonal solid solution concentration range is not more than several mol%. Hexagonal $La_{0.3}Y_{0.7}PO_4{\cdot}nH_2O$ solid solution, and a series of monoclinic $La_{1-x}Y_xPO_4$ solid solutions obtained by calcination of initial hexagonal compositions were investigated in [18, 24]. According to this research, heat treatment at 950 °C caused the decomposition of hexagonal $La_{0.3}Y_{0.7}PO_4{\cdot}nH_2O$ solid solution into a monoclinic $La_{1-x}Y_xPO_4$ solid solution and tetragonal YPO_4. The solid solubility of Y in $LaPO_4$ in the 1000 – 1600 °C temperature range increases from ~12 at. % at 1000 °C to ~42 at. % at 1600 °C [18].

The purpose of this work is to increase the mutual solubility of initial components in the case of nanosized $LaPO_4$-YPO_4-H_2O and $LaPO_4$-$LuPO_4$-H_2O systems and to investigate physicochemical properties of nanosized solid solutions and their mixtures.

II. Experimental

The initial reagents for lanthanum-yttrium and lanthanum-lutetium orthophosphates were La_2O_3 (LaO-D OST 48 – 194 – 81, 99.999 %), Y_2O_3 (ItO-Lyum OST 48 – 4-191 – 72, 99.999 %), and Lu_2O_3 (LyuO-D OST 48 – 207 – 81, 99.999 %), monosubstituted ammonium phosphate (special-purity grade, 99.5 %), nitric acid (special-purity grade, 70 %), aqua ammonia (special-purity grade, 25 %), and distilled water.

Synthesis of $La_{1-x}Y_xPO_4 \cdot nH_2O$ and $La_{1-x}Lu_xPO_4 \cdot nH_2O$ nanoparticles was performed with a conventional technique according to following reaction:

$$(1\text{-}x)Ln'_2O_3 + xLn''_2O_3 + 6HNO_3 \rightarrow 2Ln'_{1-X}Ln''_X(NO_3)_3 + 3H_2O$$

$$2Ln'_{1-X}Ln''_X(NO_3)_3 + 2NH_4H_2PO_4 \rightarrow 2Ln'_{1-X}Ln''_XPO_4^- + 2NH_4NO_3 + 4HNO_3,$$

where Ln' = La; Ln" = Y, Lu.

Proper pH ≈ 7 for complete precipitation was reached with NH_4OH addition. The precipitates were kept in the mother liquor for 24 h, then washed by means of decantation, filtered off, and dried at 110 °C in air for 24 h [16, 17, 25].

For x-ray powder diffraction analysis a Siemens D-500HS x-ray diffractometer (Germany) and DRON-3 diffractometer (Russia) were used. The recording parameters were the following: Ni-filtered CuK_α radiation, 38 kV, time constant 1, scanning speed 1 degree per minute.

Nanoparticle size was determined from the broadening of the diffraction peaks according to Scherrer 's formula and with the use of transmission electron microscopy (EM-125 electron microscope, Russia, U_{acc} = 75 kV).

Temperature dependence of nanoparticle size was determined in the temperature range of 200 – 1100 °C with isothermal exposure for 1 h.

The specific surface area of powder samples was measured with a Nova 1200e instrument (Quantachrome, USA) using nitrogen (99.9999 %) as adsorbing gas. All calculations were performed using the NovaWIN (Quantachrome, USA) 11 software. Degassing procedure was performed at 300 °C for 10 h.

The thermal behavior of the samples was studied by means of stepwise heating of powders compacted into tablets under 8 – 10 MPa pressure in the 200 – 1000 °C temperature range with further analysis with XRD or differential scanning calorimetry (DSC) and thermal gravimetry (TG).

The DSC/TG measurements were conducted in a STA 449C (Netzsch) calorimeter; sample mass was about 30 mg; heating rate was 10 °C/min. The onset of the thermal effect was determined from the intersection of the tangents to the base line of the DSC curve and to the branch of the thermal peak.

The melting temperatures of the samples of the $LaPO_4$-YPO_4 system were determined using visual polythermal analysis (VPA) in Galakhov's modified microfurnace [26, 27, 28]. The working temperature range in the microfurnace was 900 – 2300 °C. Temperature measurement accuracy was about ±(10 – 15) K. The measurements were conducted in an inert atmosphere (argon) at a total pressure in the system of about 0.5 MPa. To avoid active interaction between a specimen and a holder, the latter was produced from iridium.

III. Results and Discussion

$La_{1-x}Y_xPO_4{\cdot}nH_2O$ (x = 0.0, 0.1, 0.25, 0.3, 0.4, 0.5, 0.6, 0.7, 0.75, 0.8, 0.85, 0.9, 0.95 and 1.0) and $La_{1-x}Lu_xPO_4{\cdot}nH_2O$ (x = 0.0, 0.25, 0.3, 0.4, 0.5, 0.6, 0.7, 0.75, 0.8, 0.9 and 1.0) nanopowders were synthesized with the technique described above.

The XRD patterns of the $La_{1-x}Y_xPO_4{\cdot}nH_2O$ and $La_{1-x}Lu_xPO_4{\cdot}nH_2O$ samples thus obtained are shown in Figs. 1 and 2. They indicate that the powders are nanoscaled, and at temperature of synthesis (room temperature) limited solid solutions are formed.

Substitutional solid solutions based on hexagonal $LaPO_4{\cdot}nH_2O$ extend to concentration of Y^{3+} approximately of x = 0.5(0.7) (Fig. 1, *1 – 5(7)*), and solid solutions based on tetragonal $YPO_4{\cdot}nH_2O$ are observed in a narrow concentration range (Fig. 1, *9 – 12*). Unfortunately, nanoparticle size of specimens in the $0.4 \le x \le 1.0$ concentration range is so small that x-ray patterns do not allow precise determination of reflexes belonging to these or those solid solutions.

X-ray patterns of $La_{1-x}Lu_xPO_4{\cdot}nH_2O$ samples shown in Fig. 2 allow assumption of an extension of hexagonal solid solutions approximately to x = 0.5 – 0.6 (Fig. 2, *1 – 6*). Solubility of $LaPO_4{\cdot}nH_2O$ in $LuPO_4{\cdot}nH_2O$ at room temperature is difficult to assess owing to very broad reflexes with low intensity (Fig. 2, *7 – 9*).

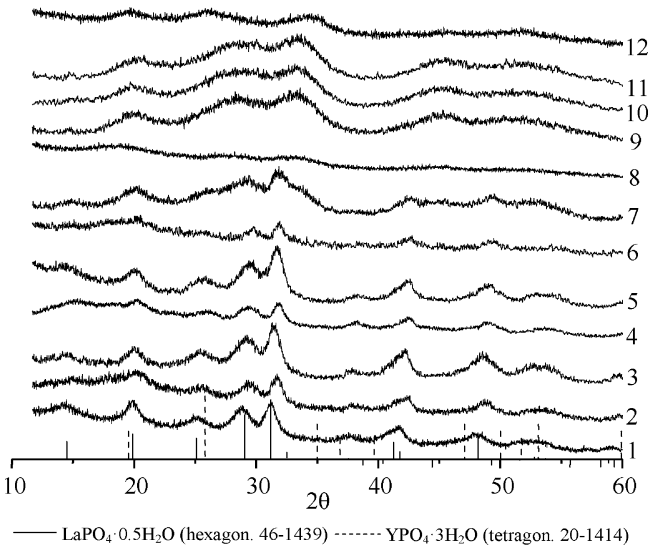

Fig. 1: XRD patterns of initial $La_{1-x}Y_xPO_4 \cdot nH_2O$ samples, *x*: 0.0 (*1*), 0.25 (*2*), 0.3 (*3*), 0.4 (*4*), 0.5 (*5*), 0.6 (*6*), 0.7 (*7*), 0.75 (*8*), 0.8 (*9*), 0.85 (*10*), 0.9 (*11*) 1.0 (*12*), and the bar graphs represent the XRD patterns of $LaPO_4 \cdot 0.5H_2O$ and $YPO_4 \cdot 3H_2O$ of ICDD-PDF.

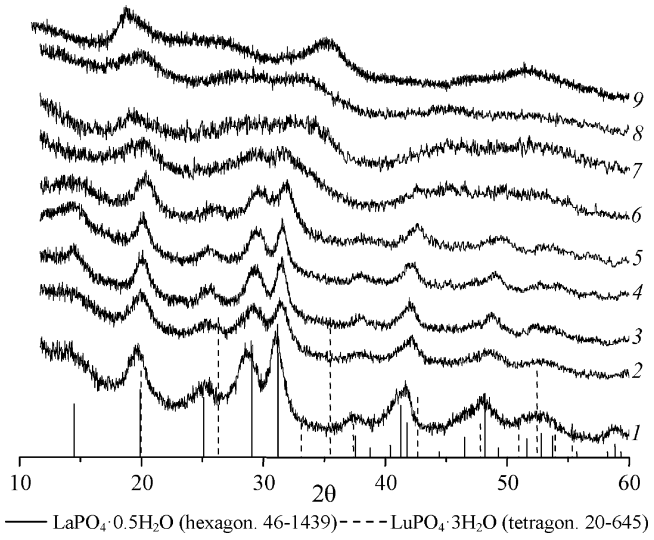

Fig. 2: XRD patterns of initial $La_{1-x}Lu_xPO_4 \cdot nH_2O$ samples, *x*: 0.0 (*1*), 0.25 (*2*), 0.3 (*3*), 0.4 (*4*), 0.5 (*5*), 0.6 (*6*), 0.7 (*7*), 0.75 (*8*), 1.0 (*9*), and the bar graphs represent the XRD patterns of $LaPO_4 \cdot 0.5H_2O$ and $LuPO_4 \cdot 3H_2O$ of ICDD-PDF.

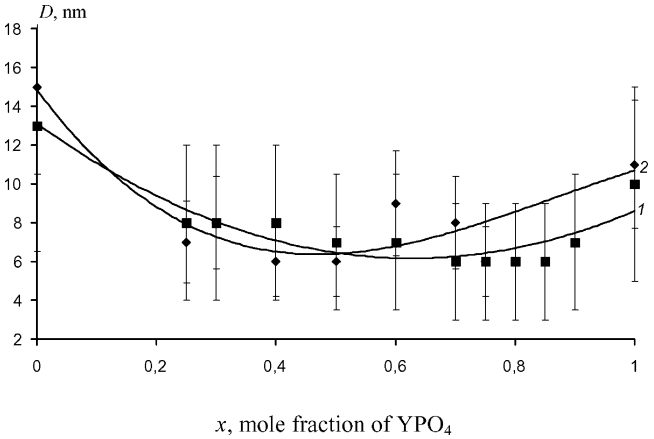

Fig. 3: Dependence of nanoparticle size (*D*) of initial $La_{1-x}Y_xPO_4 \cdot nH_2O$ samples on *x* according to (*1*) X-ray powder diffraction and (*2*) electron microscopy.

The data obtained from x-ray powder diffraction (Figs. 3, 4, curve *1*) and transmission electron microscopy (Figs. 3, 4, curve *2*) indicate the nanoscale $La_{1-x}Y_xPO_4 \cdot nH_2O$ and $La_{1-x}Lu_xPO_4 \cdot nH_2O$ particles. In addition, according to electron microscopy, the samples under investigation consist of nanoparticles in the form of rods ($LaPO_4 \cdot nH_2O$) or thin plates ($La_{1-x}Y_xPO_4 \cdot nH_2O$ and $La_{1-x}Lu_xPO_4 \cdot nH_2O$), and of a great amount of sufficiently large agglomerates (Fig. 5).

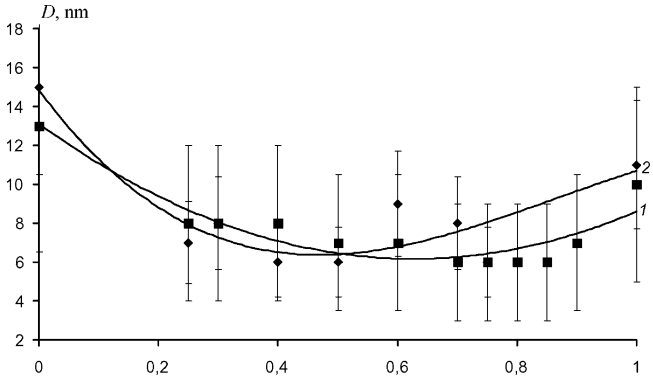

Fig. 4: Dependence of nanoparticle size (*D*) of initial $La_{1-x}Lu_xPO_4 \cdot nH_2O$ samples on *x* according to (*1*) X-ray powder diffraction and (*2*) electron microscopy.

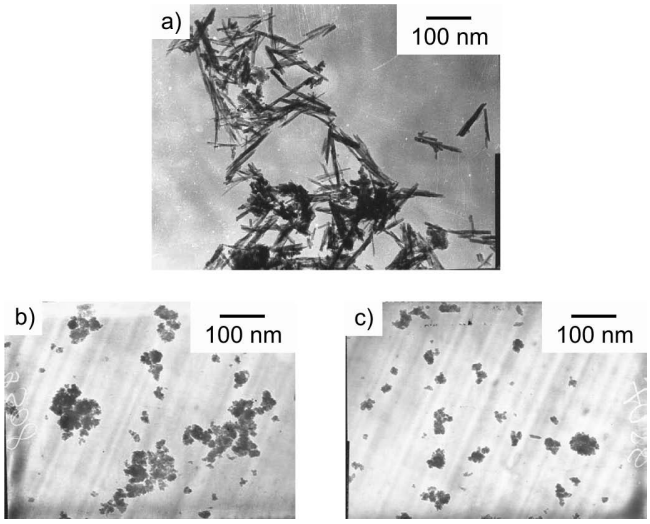

Fig. 5: Micrographs of nanocrystals: (*a*) $LaPO_4 \cdot nH_2O$, (*b*) $La_{0.75}Y_{0.25}PO_4 \cdot nH_2O$ and $La_{0.75}Lu_{0.25}PO_4 \cdot nH_2O$ (*c*) prepared at room temperature.

When heated, hexagonal $LaPO_4 \cdot nH_2O$ and its solid solutions in 500–600 °C temperature range transform into monoclinic form (Figs. 6, 7) stable until at least 1000–1100 °C (Figs. 8, 9). Isomorphic capacity of monoclinic $LaPO_4$ therefore appeared to be 70 mol% of YPO_4, and not more than 25 mol% of $LuPO_4$. Solubility of $LaPO_4$ in tetragonal YPO_4 and $LuPO_4$ is obviously less than 10 mol%.

The lattice parameters determined at room temperature (PDWin program) from the broadening of the diffraction peaks according to the Scherrer formula for monoclinic

$La_{1-x}Y_xPO_4$ series calcined at 1000 °C (1 h) are presented in [29]. The concentration dependence of unit cell parameters confirms, in our opinion, 70 mol% isomorphic capacity of monoclinic $LaPO_4$ at 1000 °C in respect of YPO_4.

The concentration dependence of monoclinic $La_{1-x}Lu_xPO_4$ unit cell parameters apparently shows the monoclinic $LaPO_4$ isomorphic capacity at about 20 mol% (Fig. 10). This is in agreement with Y^{3+} and Lu^{3+} ionic radii for coordination number 8 (0.116 and 0.112 nm respectively).

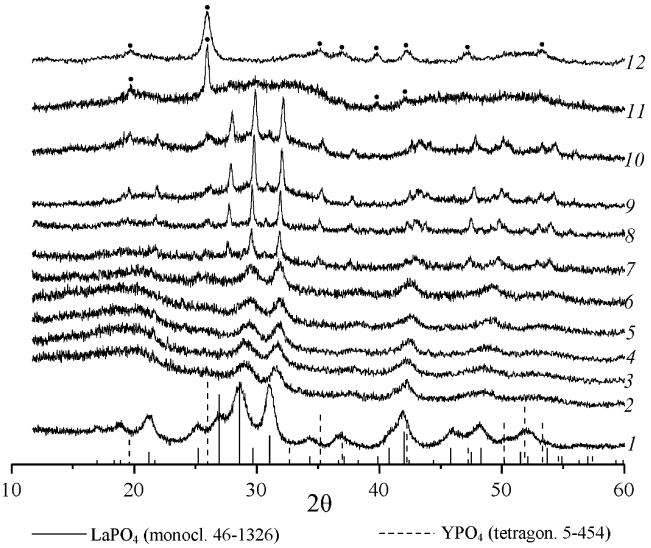

Fig. 6: XRD patterns of $La_{1-x}Y_xPO_4$ samples after heating at 600 °C for 1 h, *x*: 0.0 (*1*), 0.25 (*2*), 0.3 (*3*), 0.4 (*4*), 0.5 (*5*), 0.6 (*6*), 0.7 (*7*), 0.75 (*8*), 0.8 (*9*), 0.85 (*10*), 0.9 (*11*) 1.0 (*12*), and the bar graphs represent the XRD patterns of $LaPO_4$ and YPO_4 of ICDD-PDF – tetragonal phase.

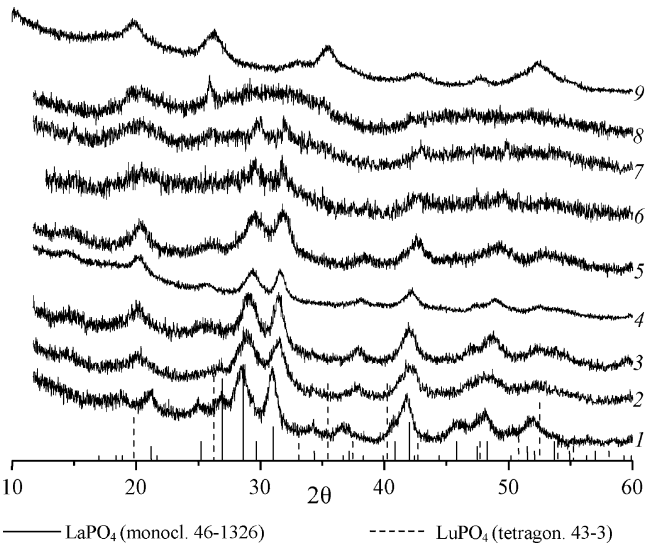

Fig. 7: XRD patterns of $La_{1-x}Lu_xPO_4$ samples after heating at 600 °C for 1 h, *x*: 0.0 (*1*), 0.25 (*2*), 0.3 (*3*), 0.4 (*4*), 0.5 (*5*), 0.6 (*6*), 0.7 (*7*), 0.75 (*8*), 1.0 (*9*), and the bar graphs represent the XRD patterns of $LaPO_4$ and $LuPO_4$ of ICDD-PDF.

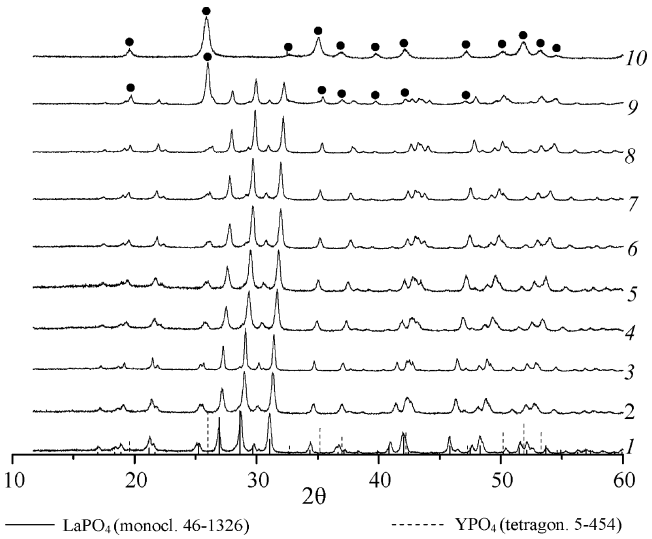

Fig. 8: XRD patterns of $La_{1-x}Y_xPO_4$ samples after heating at 1000 °C for 1 h, *x*: 0.0 (1), 0.25 (2), 0.3 (3), 0.5 (4), 0.6 (5), 0.7 (6), 0.8 (*7*), 0.85 (8), 0.9 (9), 1.0 (10), and the bar graphs represent the XRD patterns of $LaPO_4$ and YPO_4 of ICDD-PDF – tetragonal phase.

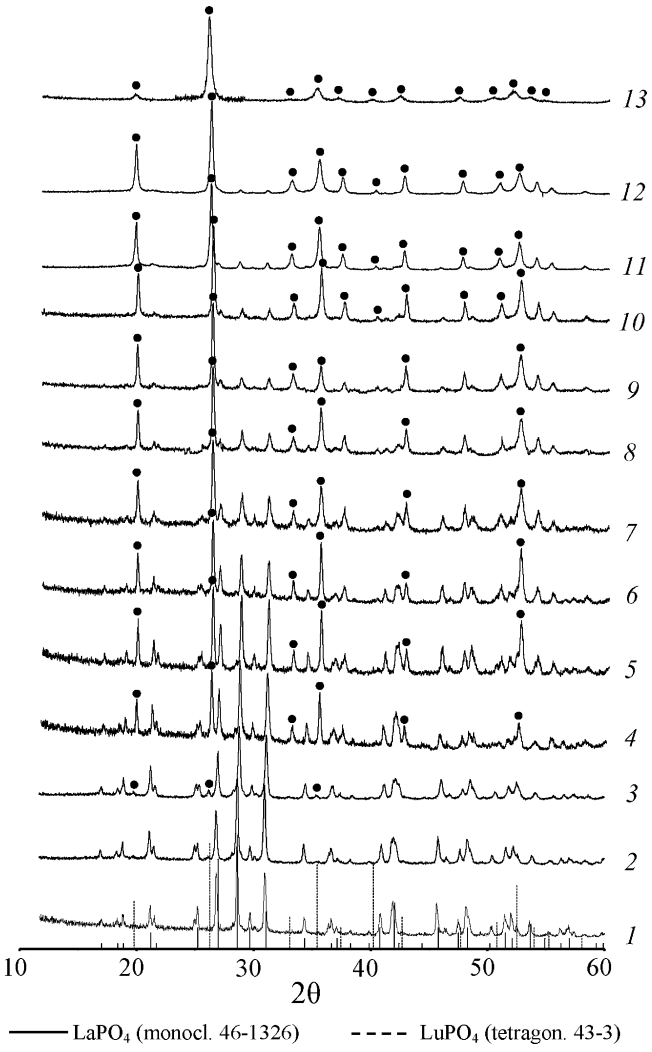

Fig. 9: XRD patterns of $La_{1-x}Lu_xPO_4$ samples after heating at 1100 °C for 1 h, *x*: 0.0 (*1*), 0.1 (*2*), 0.2 (*3*). 0.25 (*4*), 0.3 (*5*), 0.4 (*6*), 0.5 (*7*), 0.6 (*8*), 0.7 (*9*), 0.75 (*10*), 0.8 (*11*). 0.9 (*12*). 1.0 (*13*), and the bar graphs represent the XRD patterns of $LaPO_4$ and $LuPO_4$ of ICDD-PDF – tetragonal phase (main lines).

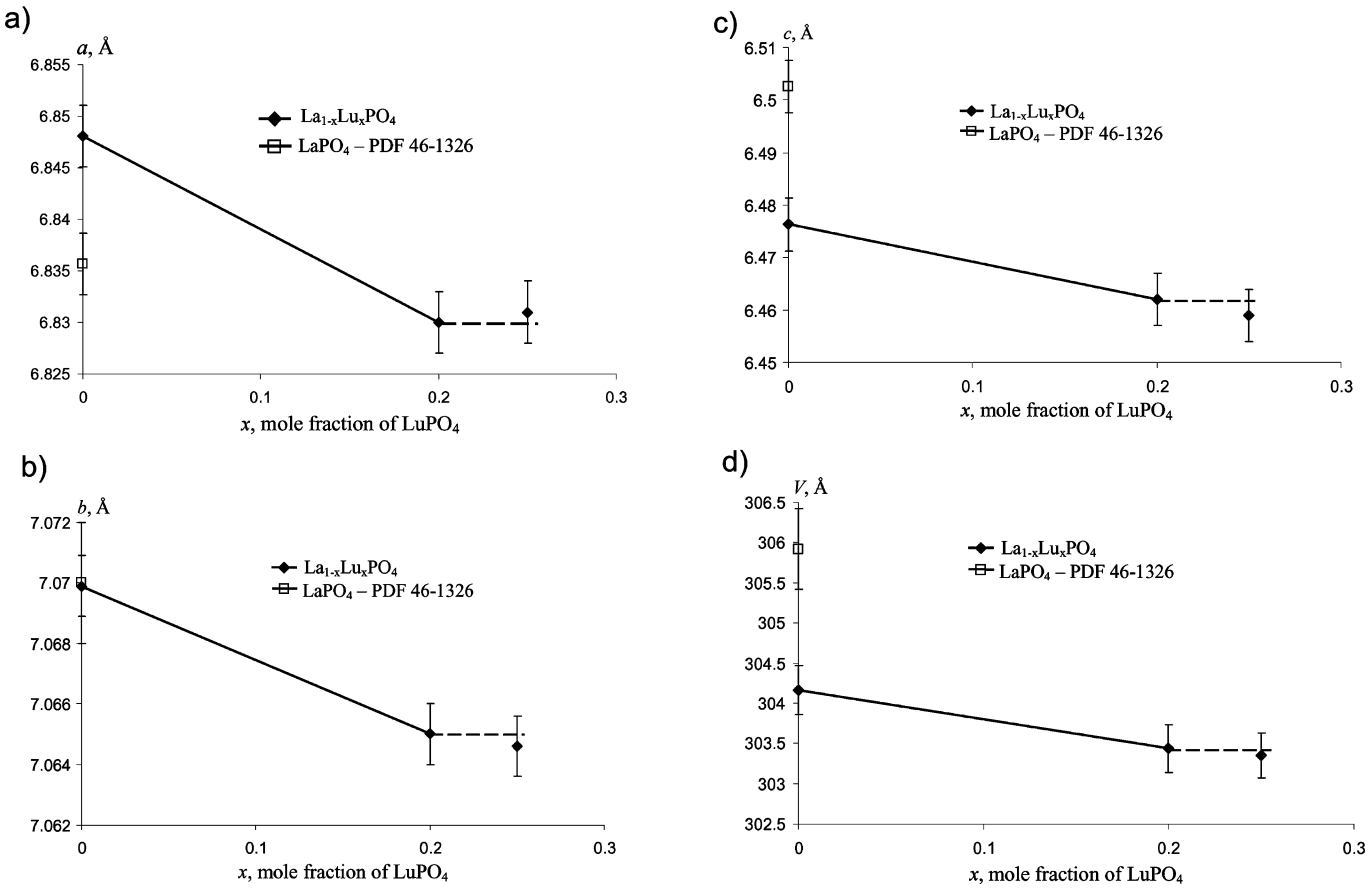

Fig. 10: Unit cell parameters of a monoclinic $La_{1-x}Lu_xPO_4$ series of samples calcined at 1000 °C (1 h): (*a*) – parameter *a*, Å; (*b*) – parameter *b*, Å; (*c*) – parameter *c*, Å; (*d*) – volume *V*, Å^3.

Fig. 11 presents the DSC/TG curves of the $La_{1-x}Y_xPO_4{\cdot}nH_2O$ samples at various yttrium concentrations (*x*). If these curves are compared with the curves given in [17] for the $La_{1-x}Lu_xPO_4{\cdot}nH_2O$ series, we can say that they illustrate the existence of two types of solid solutions with very similar thermal behavior for each type (endothermic effects observed in the range of 90 – 400 °C and the considerable weight loss of the samples is associated with water removal [17, 19, 20, 21, 22, 24, 25, 30]).

Weak exothermic effects with onset in the range of 425 – 485 °C observed for the samples with Lu^{3+} content up to $x = 0.5 – 0.6$ can be referred to monotropic hexagonal-monoclinic phase transformation according to [17, 19] and Fig. 7. A $LaPO_4{\cdot}nH_2O$ sample usually does not reveal this effect [31].

In case of $La_{1-x}Y_xPO_4{\cdot}nH_2O$ samples, these weak exothermic effects based on monotropic hexagonal-monoclinic phase transformation are observed in the range of 420 – 480 °C up to $x = 0.7 – 0.75$.

At higher temperatures exothermic effects appear on the DSC curves of both the $La_{1-x}Y_xPO_4{\cdot}nH_2O$ (Fig. 11) and $La_{1-x}Lu_xPO_4{\cdot}nH_2O$ series of samples [17, 25] which are not accompanied by mass loss.

In particular, a $La_{1-x}Y_xPO_4{\cdot}nH_2O$ series shows exothermic effects in 613 – 690 °C temperature range. At Y^{3+} concentration of $x = 0.6$, a weak broadened effect appears at 690 °C. Then at Y^{3+} content of $x = 0.7 – 0.75$ double exothermic effects appear with onset at 616 and 678 °C, and 618 and 677 °C respectively. In the case of $YPO_4{\cdot}nH_2O$, a weak broadened effect is observed at 613 °C.

A similar phenomenon takes place in the case of $La_{1-x}Lu_xPO_4{\cdot}nH_2O$ samples [17]. In $0.6 \le x \le 0.75$ concentration range of Lu^{3+} double exothermic effects appear, namely at 715 and 790 °C for $x = 0.6$, 725 and 795 °C for $x = 0.7$, 760 and 840 °C for $x = 0.75$. In the case of $LuPO_4{\cdot}nH_2O$ a weak broadened effect is observed at 570 °C.

The size effect of orthophosphates is noticeable in the general run of DSC curves, especially for the samples containing tetragonal phase [16, 17, 25]. Thus on DSC curves the onset of the exothermal effects is observed at 600 – 700 °C (Fig. 11, curves *6 – 9*), and was not observed for micron-size particles of Ho, Tm, Er, Yb, Lu and Y orthophosphates [21, 30, 32, 33, 34] and considered to be associated with intensification of nanograin growth process (Figs. 12, 13).

Temperature dependences of the particle sizes *D* versus concentrations *x* for $La_{1-x}Lu_xPO_4(\cdot nH_2O)$ samples clearly illustrate an existence of two types of solid solutions (monoclinic and tetragonal). In the case of $La_{1-x}Y_xPO_4$ $(\cdot nH_2O)$ this is not so obvious, very likely due to a narrower concentration range for the coexistence of the two solid solutions (Figs. 12, 13).

Specific surfaces for $La_{1-x}Lu_xPO_4(\cdot nH_2O)$ samples compared with literature data and melting temperatures of $La_{1-x}Y_xPO_4$ samples are presented in Table 1 and Table 2, respectively.

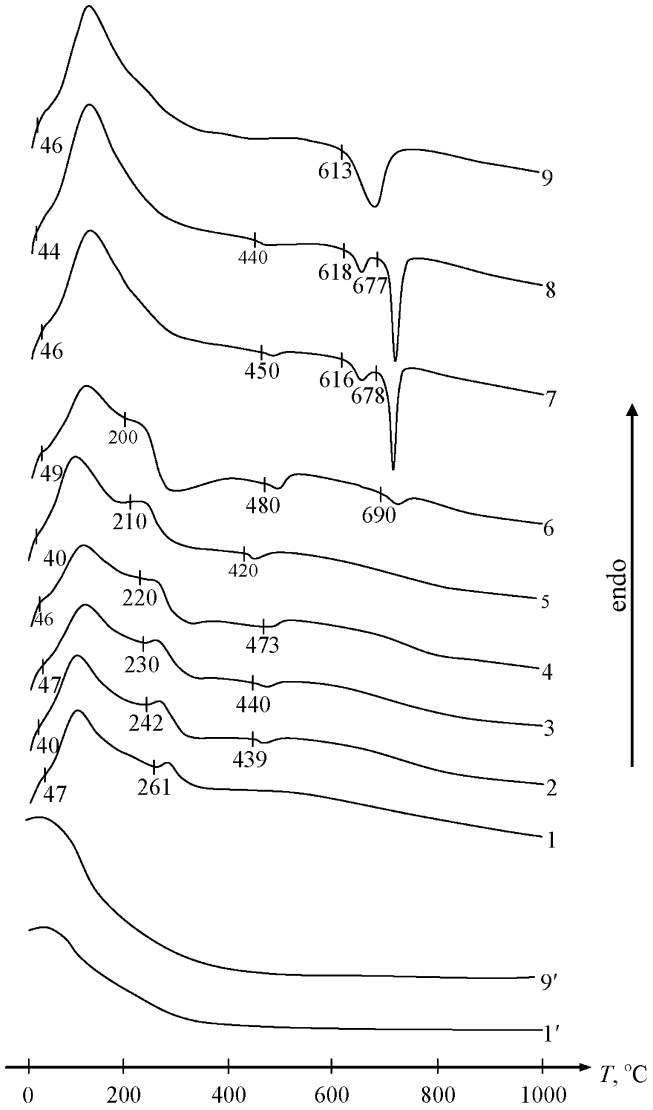

Fig. 11: DSC curves for the $La_{1-x}Y_xPO_4 \cdot nH_2O$ samples at yttrium concentrations x: 0.0 (*1*), 0.25 (*2*), 0.3 (*3*), 0.4 (*4*), 0.5 (*5*), 0.6 (*6*), 0.7 (*7*), 0.75 (*8*), 1.0 (*9*). TG curves for $LaPO_4 \cdot nH_2O$ (*1'*) and $YPO_4 \cdot nH_2O$ (*9'*) samples.

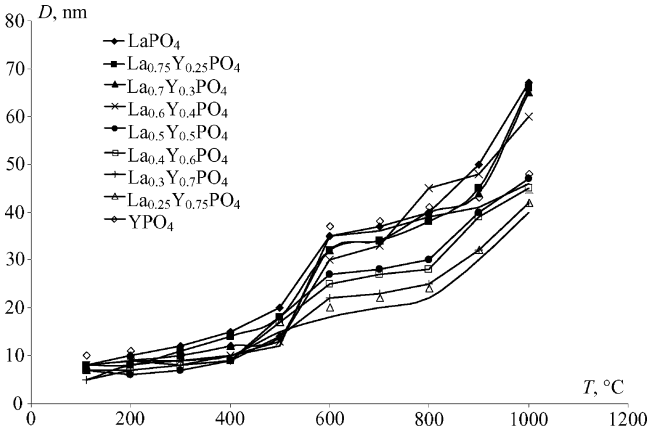

Fig. 12: Dependences of the average particle size D on the calcination temperature (1 h) for the $La_{1-x}Y_xPO_4 \cdot nH_2O$ samples at various yttrium concentrations x (within experimental and estimating error of about 50 % for Scherrer's formula and about 30 % for electron microscopy).

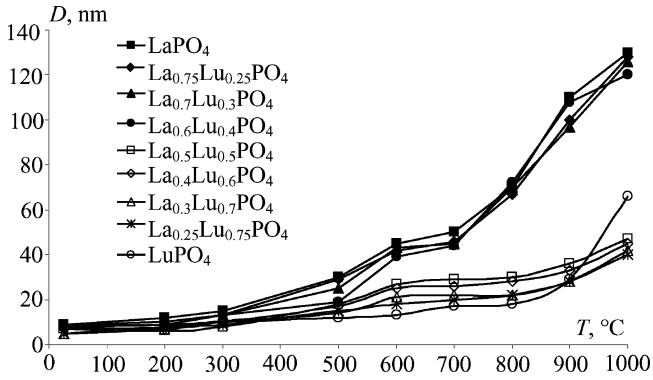

Fig. 13: Dependences of the average particle size D on the calcination temperature (1 h) for the $La_{1-x}Lu_xPO_4 \cdot nH_2O$ samples at various lutetium concentrations x (within experimental and estimating error of about 50 % for Scherrer's formula and about 30 % for electron microscopy).

Table 1: Specific surface area of $La_{1-x}Lu_xPO_4 \cdot nH_2O$ powders determined with the multipoint BET method compared with literature data for $LaPO_4 \cdot nH_2O$.

Sample, x	Crystal structure	Specific surface area, m^2/g	Specific surface area, m^2/g (from literature)
0.0	Hexagonal	62.0	55 – 97 [34], 76 [35]
0.25	Hexagonal	90.3	–
0.3	Hexagonal	66.7	–
0.4	Hexagonal	64.6	–
0.5	Hexagonal	53.8	–
0.6	Hexagonal	46.7	–
0.7	Hexagonal	61.1	–
0.75	Hexagon. + tetragon.	63.5	–
1.0	Tetragonal	3.3	–

Table 2: Melting temperatures of $La_{1-x}Y_xPO_4$ samples determined by using VPA in Galakhov's modified microfurnace (argon, total pressure in the system – 0.5 MPa)

Sample, x	Crystal structure	Melting temperature, (± (10 – 15 K))
0.0	Monoclinic	2050
0.25	Monoclinic	2010
0.3	Monoclinic	2040
0.4	Monoclinic	1987
0.5	Monoclinic	1984
0.6	Monoclinic	1993
0.7	Monoclinic	1985
0.75	Monocl. + tetragon.	1960
1.0	Tetragonal	1980

IV. Summary

The synthesized individual orthophosphates ($LnPO_4 \cdot nH_2O$) and their binary compositions in $LaPO_4$-YPO_4-H_2O and $LaPO_4$-$LuPO_4$-H_2O systems are nanodispersed, with an average grain size of 10 – 20 nm and high specific surface area of hexagonal samples.

Three types of solid solutions were found in the systems – hexagonal, monoclinic and tetragonal.

In the $LaPO_4$-YPO_4(-H_2O) system, a series of limited hexagonal solid solutions based on $LaPO_4 \cdot nH_2O$ is observed up to 500 – 600 °C within the $0 \le x \le 0.5$ concentration range which transforms above this temperature into a monoclinic form based on $LaPO_4$ and remains up to at least 1000 °C. The isomorphic capacity of monoclinic $LaPO_4$ at 1000 °C is therefore about 70 mol%.

In the $LaPO_4$-$LuPO_4$(-H_2O) system, a series of limited hexagonal solid solutions based on $LaPO_4 \cdot nH_2O$ is observed up to the same temperatures (500 – 600 °C) within the $0 \le x \le 0.4$ concentration range. Monoclinic form in this system remains up to 1100 °C, and its isomorphic capacity at this temperature is about 20 mol%.

Solubility of $LaPO_4$ in tetragonal YPO_4 or $LuPO_4$ in all cases is less than 10 mol%.

Therefore, rare earths orthophosphate nanopowders are suitable for the preparation of ceramics for radioactive waste immobilization relating to actinide/rare-earth group occurring in high-level waste (HLW) because rare earths orthophosphates possess high chemical resistance and isomorphic capacity, as well as high thermal stability.

Melting temperatures of $La_{1-x}Y_xPO_4$ samples were found to be in the 2010 – 1960 °C temperature range, which is high enough for the purpose of radioactive waste immobilization.

Acknowledgments

The authors gratefully acknowledge the financial support by the Russian Foundation for Basic Research, Project No. 14 – 03 – 00697-a, and Department of Chemistry and Materials Sciences of Russian Academy of Sciences, the Program "Development of novel metallic, ceramic, glass-, polymeric and composite materials" for 2012 – 2014).

The authors are much obliged to Prof. A. Lapshin and Prof. R. Bubnova for discussion on some aspects of structural chemistry.

References

1 Pemba-Mabiala, J.M., Lenzi, M., Lenzi, J., Lebugle,A.: XPS study of mixed cerium-terbium orthophosphate catalysis, *Surface Interface Anal.*, **15**, 663 – 667, (1990).

2 Takita, Y., Sano, K., Muraya, T., Nishiguchi, H., Kawata, N., Ito, M., Akbay, T., Ishihara, T.: Oxidative dehydrogenation of iso-butane to iso-butene II. Rare earth phosphate catalysts, *Appl. Catalysis A: General*, **170**, 23 – 31, (1998).

3 Takita, Y., Qing, X., Takami, A., Nishiguchi, H., Nagaoka, K.: Oxidative dehydrogenation of isobutane to isobutene III Reaction mechanism over $CePO_4$ catalyst, *Appl. Catalysis A: General*, **296**, 63 – 69, (2005).

4 Jellison, G.E. Boatner, L.A., Chi, C.: Spectroscopic refractive indices of metalorthophosphates with the zircon-type structure, *Optical Mater.*, **15**, 103 – 109, (2000).

5 Riwotzki, K., Meyssamy, H., Schnablegger, H., Kornowski, A., Haase, M.: Liquid-phase synthesis of colloids and redispersible powders of strongly luminescing $LaPO_4$:Ce,Tb nanocrystals, *Angew. Chem. Int. Ed.*, **40**, 573 – 576, (2002).

6 Zhu, H., Zhu, E., Yang, H., Wang, L., Jin, D., Yao, K.: High-brightness $LaPO_4$:Ce^{3+},Tb^{3+} nanophosphors: Reductive hydrothermal synthesis and photoluminescent properties, *J. Am. Ceram. Soc.*, **91**, 1682 – 1685, (2008).

7 Davis, J.B., Marshall, D.B., Horsley, R.M., Morgan, P.E.D.: Machinable ceramics coating rare-earth phosphates, *J. Am. Ceram. Soc.*, **81**, 2169 – 2175, (1998).

8 Wang, R., Pan, W., Chen, J., Fang, M., Cao, Z., Luo, Y.: Synthesis and sintering of $LaPO_4$ powder and its application, *Mater. Chem. Phys.*, **79**, 30 – 36, (2003).

9 Boatner, L.A., Abraham, M.M., Sales, B.C.: Lanthanide orthophosphate ceramics for the disposal of actinide-contaminated nuclear wastes, *Inorg. Chim. Acta*, 94, 146 – 148, (1984).

10 Volkov, Yu. F.: Compounds with zircon and monazite structures and possibilities of their use for incorporation of radionuclides, *Radiochemistry*, **41**, 168 – 174, (1999).

11 Terra, O., Clavier, N., Dacheux, N., Podor, R.: Preparation and characterization of lanthanum-gadolinium monazites as ceramics for radioactive waste storage, *New J. Chem.*, 27, 957 – 967, (2003).

12 Ewing, R.C., Weber, W.J., Clinard, F.W.: Radiation effects in nuclear waste forms for high-level radioactive waste, *Progr. Nucl. Energ.*, **29**, 63 – 127, (1995).

13 Ivanova, O.P., Naumkin, A.V., Vasilyev, L.A.: An XPS study of compositional changes induced by argon ion bombardment of the $LaPO_4$ surface, *Vacuum*, **47**, 67 – 71, (1996).

14 ICDD-PDF No.46 – 439 ($LaPO_4 \cdot 0.5H_2O$); No.46 – 1326 ($LaPO_4$); No.20 – 1414 ($YPO_4 \cdot 3H_2O$); No.5 – 454 (YPO_4); No.20 – 654 ($LuPO_4 \cdot 3H_2O$); No.43 – 3 ($LuPO_4$).

15 Bondar', I.A., Domanskii, A.I., Mezentseva, L.P., Degen, M.G., Kalinina, N.E.: Physicochemical investigations of rare-earth orthophosphates, *Zh. Neorg. Khim.*, **21**, 2045 – 2050, (1976).

16 Osipov, A.V., Mezentseva, L.P., Drozdova, I.A., Kuchaeva, S.K., Ugolkov, V.L., Gusarov, V.V.: Crystallization and thermal transformations in nanocrystals of the YPO_4-$LuPO_4$-H_2O system, *Glass Phys. Chem.*, **33**, 169 – 173, (2007).

17 Osipov, A.V., Mezentseva, L.P., Drozdova, I.A., Kuchaeva, S.K., Ugolkov, V.L., Gusarov, V.V.: Preparation and thermal transformations of nanocrystals in the $LaPO_4$-$LuPO_4$-H_2O system, *Glass Phys. Chem.*, **35**, 431 – 435, (2009).

18 Mogilevsky, P., Boakye, E.E., Hay, R.S.: Solid solubility and thermal expansion in a $LaPO_4$-YPO_4 system, *J. Am. Ceram. Soc.*, **90**, 1899 – 1907, (2007).

19 Jonasson, R.G., Vance, E.R.: DTA study of the rhabdophane to monazite transformation in rare earth (La-Dy) phosphates, *Thermochim. Acta.*, **108**, 65 – 72, (1986).

20 Hikichi, Y., Ota, T., Hattori, T.: Thermal, mechanical and chemical properties of sintered monazite-(La, Ce, Nd or Sm), *Mineral. J.*, **19**, 123 – 130, (1997).

21 Hikichi, Y., Ota, T., Daimon, K., Hattori, T.: Thermal, mechanical, and chemical properties of sintered xenotime-type RPO_4 (R = Y, Er, Yb or Lu), *J. Am. Ceram. Soc.*, 81, 2216 – 2218, (1998).

22 Mezentseva, L.P.: Phase diagrams of the Ln_2O_3-P_2O_5 binary systems and solid solutions of rare-earth phosphates, (in Russian), *Extended Abstract of Candidate's Dissertation*, Leningrad: Institute of Silicate Chemistry of RAS, 1983, 24.

23 van Emden, B., Thornber, M.R., Graham, J., Lincoln, F.J.: Solid Solution Behaviour of Synthetic Monazite and Xenotime from Structure Refinement of Powder Data. In: Advances in X-ray Analysis, 1996, **40**, 2 – 15. Proceedings of the 45th Annual X-ray Conference, Denver, Colorado, USA, 1996.

[24] Boakye, E.E., Hay, R.S., Mogilevsky, P., Cinibulk, M.K.: Two phase monazite/xenotime $30LaPO_4$-$70YPO_4$ coating of ceramic fiber tows, *J. Am. Ceram. Soc.*, **91**, 17 – 25, (2008).

[25] Maslennikova, T.P., Osipov, A.V., Mezentseva, L.P., Drozdova, I.A., Kuchaeva, S.K., Ugolkov, V.L., Gusarov, V.V.: Synthesis, mutual solubility, and thermal behavior of nanocrystals in the $LaPO_4$-YPO_4-H_2O system, *Glass Phys. Chem.*, **36**, 351 – 357, (2010).

[26] Galakhov, F. Ya.: High-temperature microfurnace for heterogeneous equilibria investigations in refractory oxide systems, In: Modern Techniques of Silicate and Construction Materials Studies, (in Russian), Gosstroyizdat Publishers, Moscow, (1961), p. 178.

[27] Mezentseva, L.P., Popova, V.F., Al'myashev, V.I., Lomanova, N.A., Ugolkov, V.L., Beshta, S.V., Khabenskii, V.B., Gusarov, V.V.: Phase and chemical transformations in the SiO_2-Fe_2O_3(Fe_3O_4) system at various oxygen partial pressures, *Russian J. Inorgan. Chem.*, **51**, 118 – 125, (2006).

[28] Bechta, S.V., Krushinov, E.V., Almjashev, V.I., Vitol, S.A., Mezentseva, L.P., Petrov, Yu. B., Lopukh, D.B., Khabensky, V.B., Barrachin, M., Hellmann, S., Froment, K., Fischer, M., Tromm, W., Bottomley, D., Defoort, F., Gusarov, V.V.: Phase diagram of the ZrO_2-FeO system, *J. Nucl. Mater.*, **348**, 114 – 121, (2006).

[29] Mezentseva, L.P., Kruchinina, I. Yu., Osipov, A.V., Kuchaeva, S.K., Ugolkov, V.L., Popova, V.F., Pougatchiov, K.E.: Nano-sized powders of orthophosphates in the $LaPO_4$-YPO_4-H_2O system and ceramics based on them, submitted to *Glass Phys. Chem.*, **40**, 356 – 361, (2014).

[30] Horvath, I., Mezentseva, L.P., Figusch, V.: Dehydration of $GdPO_4 \cdot xH_2O$, *Chem. Zvesti*, **35**, 333 – 338, (1981).

[31] Gavrichev, K.S., Ryumin, M.A., Tyurin, A.V., Khoroshilov, A.V., Mezentseva, L.P., Osipov, A.V., Ugolkov, V.L., Gusarov, V.V.: Thermal behavior of $LaPO_4 \cdot nH_2O$ and $NdPO_4 \cdot nH_2O$ nanopowders, *J. Therm. Anal. Calorim.,* **102**, 809 – 811, (2010).

[32] Hikichi, Y., Hukuo, K., Shiokawa, J.: Synthesis of monoclinic $YPO_4 \cdot 2H_2O$ and its thermal change, *J. Chem. Soc. Jpn, Chemistry and Industrial Chemistry* (*Nippon Kagaku Kaishi*), **11**, 1634 – 1638, (1977).

[33] Kijkowska, R.: Thermal decomposition of lanthanide orthophosphates synthesized through crystallisation from phosphoric acid solution, *Thermochim. Acta*, **404**, 81 – 88, (2003).

[34] Lucas, S., Champion, E., Bregiroux, D., Bernache-Assollant, D., Audubert, F.: Rare earth phosphate powders $RePO_4 \cdot nH_2O$ (*Re*=La, Ce or Y) – Part I. Synthesis and characterization, *J. Solid State Chem.*, **177**, 1302 – 1311, (2004).

[35] Diaz-Guillén, J.A., Fuentes, A.F., Gallini, S., Colomer, M.T.: A rapid method to obtain nanometric particles of rhabdophane $LaPO_4 \cdot nH_2O$ by mechanical milling, *J. Alloy. Compd.*, **427**, 87 – 93, (2007).